Supporting Information

Examining Copper Lead Surface Alloys as Potential Catalysts for the Electrochemical Carbon Dioxide Reduction

Oliver Kratz[†] and Axel Groß[*,†]

†*Institute of Theoretical Chemistry, Ulm University, Oberberghof 7, 89081 Ulm, Germany*

‡*Helmholtz Institute Ulm (HIU) for Electrochemical Energy Storage, Helmholtzstraße 11, 89081 Ulm, Germany*

E-mail: axel.gross@uni-ulm.de

Spin and spin-unpolarized calculations

The spin polarized calculations where initialized with a high magnitude of magnetization on copper and a low magnitude on lead, carbon, oxygen, and hydrogen. Furthermore, for copper the same pseudo potentials as for the spin unpolarized calculations was used. For lead the pseudo potential, which treats the $5d^{10}6s^26p^2$ as valance electrons, was used.

Converged structures where considered the same, if the adsorbate was at the same site on the surface, the distance to the surface of the adsorbate was with in 0.1 Å and if the angle to the surface was with in 10 °. The mean difference ($E_{ads}^{unspin} - E_{ads}^{spin}$) between adsorption energies was for hydrogen $0.0046\,eV$ and for carbon monoxide $0.0058\,eV$.

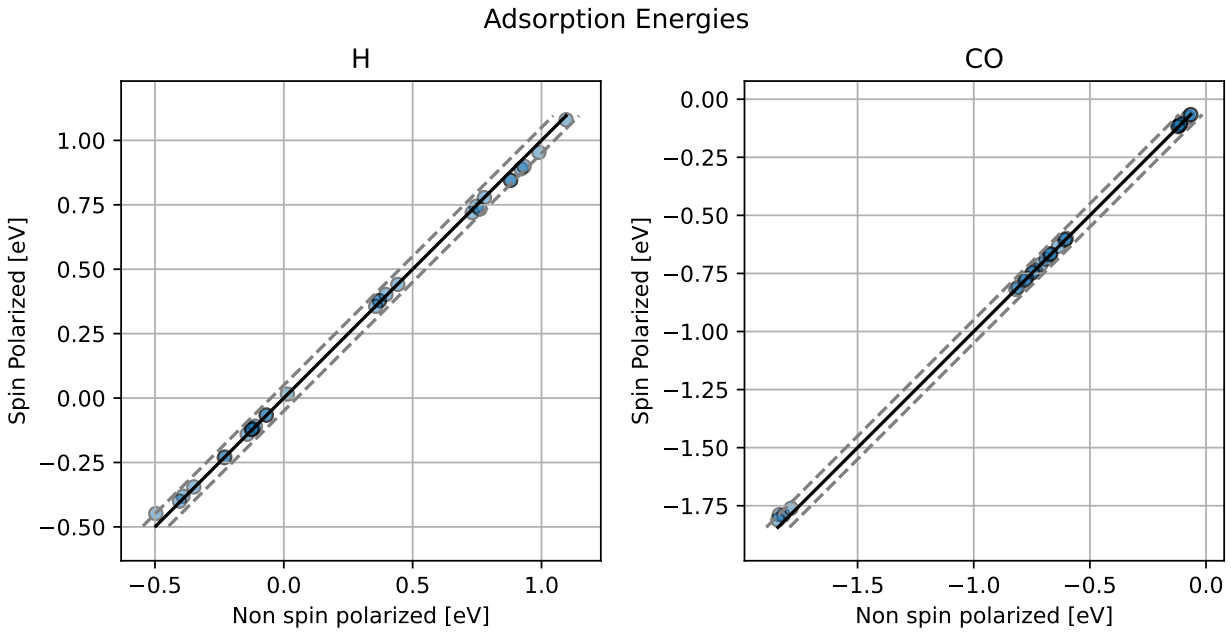


Figure S1: Adsorption energies calculated from spin polarized DFT calculations plotted against adsorption energies calculated from spin non polarized DFT calculations. The dashed gray lines are drawn at $\pm 0.05\,eV$.

Free Energy Lines

The two free energy lines in the Figures 1, 4, and 5 are drawn at $\Delta G = 0$ for the reactions $\frac{1}{2}\mathrm{H_2} \rightleftharpoons \mathrm{H^*}$ and $\mathrm{CO} \rightleftharpoons \mathrm{CO^*}$ or to be more precise $\frac{1}{2}\mathrm{H_2} + * \rightleftharpoons \mathrm{H^*}$ and $\mathrm{CO} + * \rightleftharpoons \mathrm{CO^*}$. Therefore, the lines are drawn at the border at which the adsorbate is under potential deposited.[S1] The asterisk (*) denotes adsorption of the intermediate on the surface.

The vertical solid black line is constructed from the zero point energy ($[ZPE]_{H^*}$, $[ZPE]_{\mathrm{H_2}}$), entropy ($[-TS]_{H^*}$, $[-TS]_{\mathrm{H_2}}$), and heat capacity ($[\int C_p dT]_{H^*}$, $[\int C_p dT]_{\mathrm{H_2}}$) values from Chan *et al.*[S2] and a correction of $K_{\mathrm{H_2}} = 0.09\,\mathrm{eV}$, due to functional errors in the afore mentioned values for hydrogen.[S3,S4] The vertical solid black line marks the thermodynamics of $\frac{1}{2}\mathrm{H_2} \rightleftharpoons \mathrm{H^*}$ with $\Delta G = 0$ and is drawn at $-0.2\,\mathrm{eV}$.

$$\frac{1}{2}\,\mathrm{H_2} + * \rightleftharpoons \mathrm{H^*} \tag{S1}$$

$$\begin{aligned}\Delta G = E_{H^*} + [ZPE]_{H^*} + [\int C_p dT]_{H^*} + [-TS]_{H^*} \\ - \frac{1}{2}\left(E_{\mathrm{H_2}} + [ZPE]_{\mathrm{H_2}} + [\int C_p dT]_{\mathrm{H_2}} + [-TS]_{\mathrm{H_2}} + K_{\mathrm{H_2}}\right) - E_*\end{aligned} \tag{S2}$$

$$\Delta G = 0 \tag{S3}$$

$$\begin{aligned}E_{H^*} - \frac{1}{2}E_{\mathrm{H_2}} - E_* = -\left([ZPE]_{H^*} + [\int C_p dT]_{H^*} + [-TS]_{H^*}\right) \\ + \frac{1}{2}\left([ZPE]_{\mathrm{H_2}} + [\int C_p dT]_{\mathrm{H_2}} + [-TS]_{\mathrm{H_2}} + K_{\mathrm{H_2}}\right)\end{aligned} \tag{S4}$$

$$\begin{aligned}\Delta E_{H^*} = -\left([ZPE]_{H^*} + [\int C_p dT]_{H^*} + [-TS]_{H^*}\right) \\ + \frac{1}{2}\left([ZPE]_{\mathrm{H_2}} + [\int C_p dT]_{\mathrm{H_2}} + [-TS]_{\mathrm{H_2}} + K_{\mathrm{H_2}}\right)\end{aligned} \tag{S5}$$

$$\begin{aligned}\Delta E_{H^*} &= -\left(0.23\,eV + 0.01\,eV - 0.01\,eV\right) \\ &\quad + \frac{1}{2}\left(0.28\,eV + 0.09\,eV - 0.40\,eV + 0.09\,eV\right) \\ &= -0.2\,eV\end{aligned} \tag{S6}$$

The horizontal solid black line is constructed from the zero point energy ($[ZPE]_{CO^*}$, $[ZPE]_{\mathrm{CO}}$), entropy ($[-TS]_{CO^*}$, $[-TS]_{\mathrm{CO}}$), and heat capacity ($[\int C_p dT]_{CO^*}$, $[\int C_p dT]_{CO}$) values from Chan *et al.*[S2] and a water correction for the binding energy of CO* of $K_{\mathrm{CO}^*} = 0.1\,\mathrm{eV}$.[S5] The horizontal solid black line marks the thermodynamics of $\mathrm{CO} \rightleftharpoons \mathrm{CO}^*$ with $\Delta G = 0$ and is drawn at $-0.4\,\mathrm{eV}$.

$$\mathrm{CO} + * \rightleftharpoons \mathrm{CO}^* \tag{S7}$$

$$\begin{aligned}\Delta G = E_{CO^*} + [ZPE]_{CO^*} + [\int C_p dT]_{CO^*} + [-TS]_{CO^*} + K_{\mathrm{CO}^*} \\ - \left(E_{\mathrm{CO}} + [ZPE]_{\mathrm{CO}} + [\int C_p dT]_{CO} + [-TS]_{\mathrm{CO}}\right) - E_*\end{aligned} \tag{S8}$$

$$\Delta G = 0 \tag{S9}$$

$$\begin{aligned}E_{CO^*} - E_{\mathrm{CO}} - E_* = -\left([ZPE]_{CO^*} + [\int C_p dT]_{CO^*} + [-TS]_{CO^*} + K_{\mathrm{CO}^*}\right) \\ + \left([ZPE]_{\mathrm{CO}} + [\int C_p dT]_{\mathrm{CO}} + [-TS]_{\mathrm{CO}}\right)\end{aligned} \tag{S10}$$

$$\begin{aligned}\Delta E_{CO^*} = &-\left([ZPE]_{CO^*} + [\int C_p dT]_{CO^*} + [-TS]_{CO^*} + K_{\mathrm{CO}^*}\right) \\ &+ \left([ZPE]_{\mathrm{CO}} + [\int C_p dT]_{\mathrm{CO}} + [-TS]_{\mathrm{CO}}\right)\end{aligned} \tag{S11}$$

$$\begin{aligned}\Delta E_{CO^*} &= -\left(0.19\,eV + 0.08\,eV - 0.16\,eV - 0.1\,eV\right) \\ &\quad + \left(0.13\,eV + 0.09\,eV - 0.61\,eV\right) \\ &= -0.4\,eV\end{aligned} \tag{S12}$$

Probed Adsorption Sites

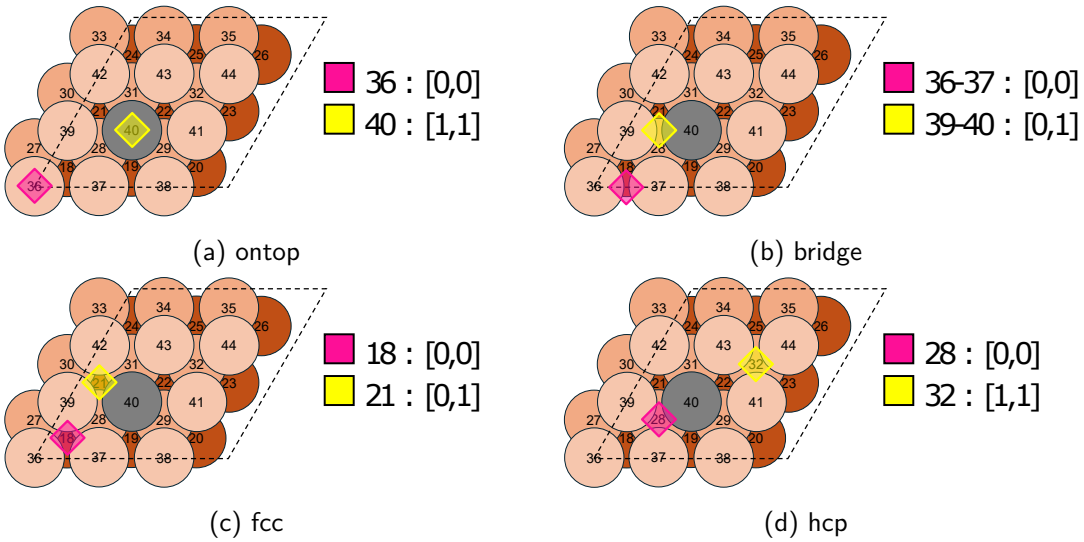


Figure S2: Scanned calculation starting positions of adsorption sites for surface alloy pattern $Pb_1Cu_8(3 \times 3)/Cu(111)$. Compared to the un-alloyed metal there are twice as many adsorption sites considered for each adsorption site type: ontop, bridge, fcc and hcp.

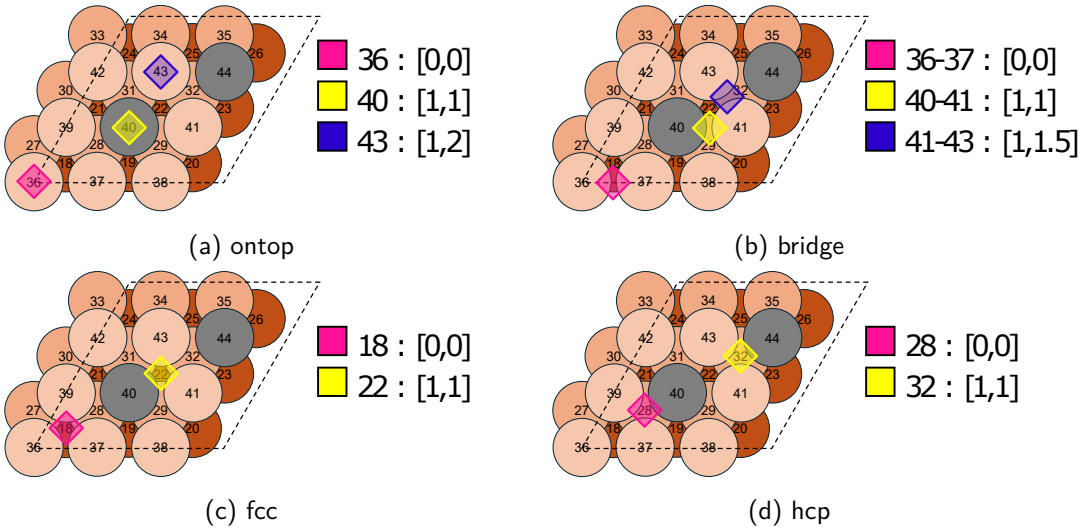


Figure S3: Scanned calculation starting positions of adsorption sites for surface alloy $Pb_2Cu_7(3 \times 3)$-hex/Cu(111). Compared to the un-alloyed metal there are more than twice as many adsorption sites considered for each adsorption site type: ontop, bridge, fcc and hcp.

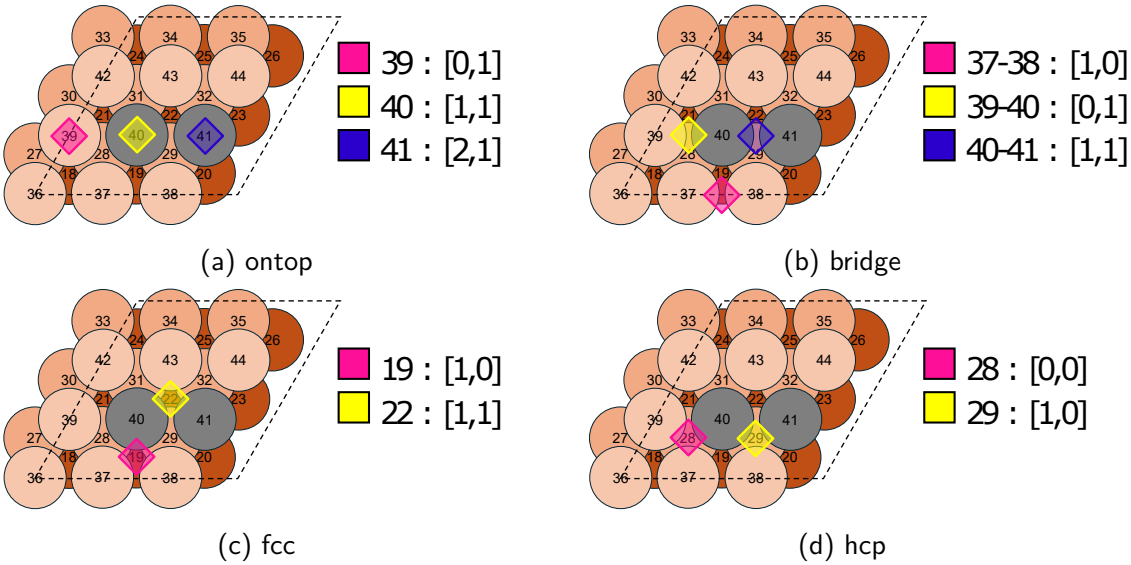


Figure S4: Scanned calculation starting positions of adsorption sites for surface alloy $Pb_2Cu_7(3 \times 3)$-dimer/Cu(111). Compared to the un-alloyed metal there are twice as many adsorption sites considered for each adsorption site type: ontop, bridge, fcc and hcp.

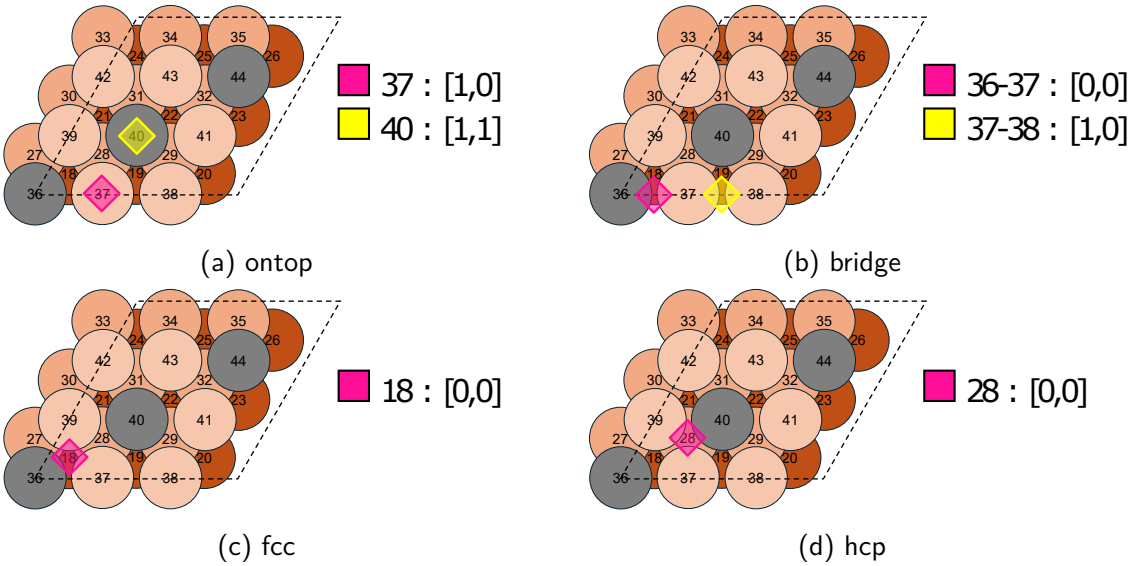


Figure S5: Scanned calculation starting positions of adsorption sites for surface alloy $Pb_3Cu_6(\sqrt{3} \times \sqrt{3})/Cu(111)$. Compared to the un-alloyed metal there are only two more adsorption sites considered.

Results for the *d*-band Center

To assess whether the d-band center can serve as a reliable descriptor for adsorption energy, the local density of states (LDOS) was analyzed for each adsorption site. The LDOS has been calculated for all surface atoms, for all surface alloy patterns examined, for copper doped with lead. The LDOS and their d-band center is of interest as it can be used to deepen the understanding of adsorption processes. If a correlation between the d-band center and adsorption energies of hydrogen and carbon monoxide could be found, identifying suitable catalyst surfaces could be computationally far less demanding.

$$e_{d\ site} = \sum_{i=1}^{N_{site}} \frac{1}{N_{site}}\ e_{d\ of\ atom\ i} \qquad \text{(S13)}$$

$$N_{ontop} = 1;\ N_{bridge} = 2;\ N_{fcc} = 3;\ N_{hcp} = 4$$

To check if there is a correlation between d-band center and adsorption energies for each site a d-band center has to be calculated. For adsorption sites where the adsorbate interacts with more than one atom the mean of the d-band center of all involved atoms was chosen

according to equation S13.

Looking at the data for the configurations of copper doped with lead (cf. fig. S6) there is no significant correlation of the d-band center with the adsorption energy. In the plot of carbon monoxide on copper atoms in a copper lead system (cf. fig. S6 top right) two distinct clusters can be seen. The average carbon monoxide distance to the surface in the top cluster is 1.61 Å with a standard deviation of 0.17 Å and in the bottom cluster the average distance is 4.33 Å with a standard deviation of 0.41 Å. The distance is defined as the difference along the z-axis between the atom of the adsorbed molecule that is closest to the surface and the mean of the non dopant surface atoms, where the z-axis is the axis orthogonal to the surface.

Taking a closer look at the d-band LDOS of lead in the various copper doped with lead surface alloy configurations (cf. S7), we would expect a strong peak at low energy for the d-electrons, as the d-orbitals are completely filled. They would lie low in energy and would not participate in bonding, which makes them have a sharp peak. This is the case, however, the d-band center is not observed to be in the center of this peak. Further analysis of the d-band structure, revealed there is a broad and shallow d-band density around $-4\,\mathrm{eV}$ to $-2\,\mathrm{eV}$ and around $4\,\mathrm{eV}$ to $6\,\mathrm{eV}$. The first of these discovered densities is exactly where the d-density of copper is the highest, suggesting it is a small bonding contribution. The second discovered density should then be the corresponding anti-bonding density, which is not populated as it is above the Fermi level.

Not finding a significant connection between adsorption energy and d-band center is not unexpected as the d-band center went from being used to predict adsorption energies to being used for more of a qualitative understanding. Furthermore, the d-band center was developed for transition metals and the systems considered are surface alloys between a transition metal and a metal from the p-block.

Overall, the analysis suggests that while the d-band center remains a useful conceptual tool, it is inadequate as a quantitative descriptor for adsorption in copper and lead alloys. The density of states plots did still bring insights, as it was found the low laying d-orbitals

of lead actually have a small bonding contribution in the copper doped with lead surface alloys.

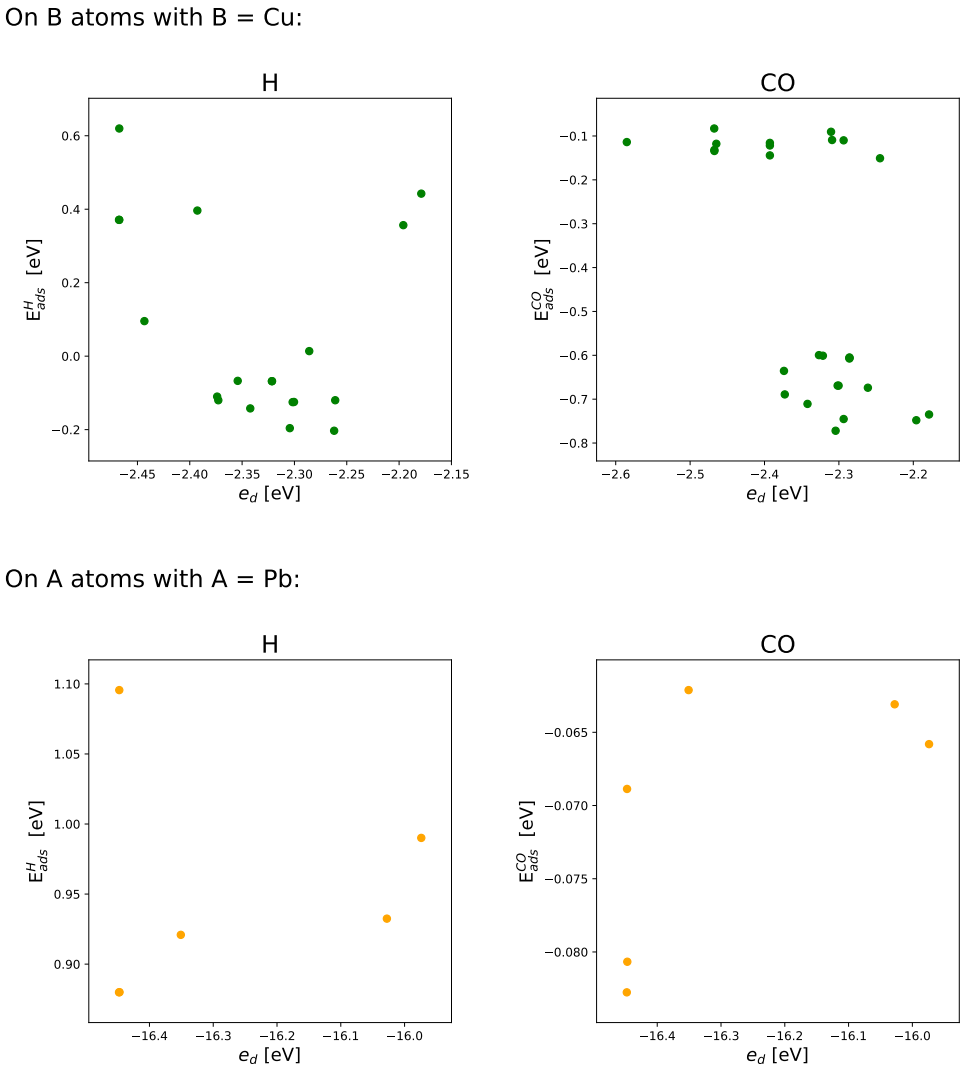


Figure S6: Adsorption energy plotted against the d-band center of the local DOS of surface atoms of the copper doped with lead surface alloy configurations. The color indicates the element, green for copper and orange for lead. Only sites comprised of a single metal type have been plotted.

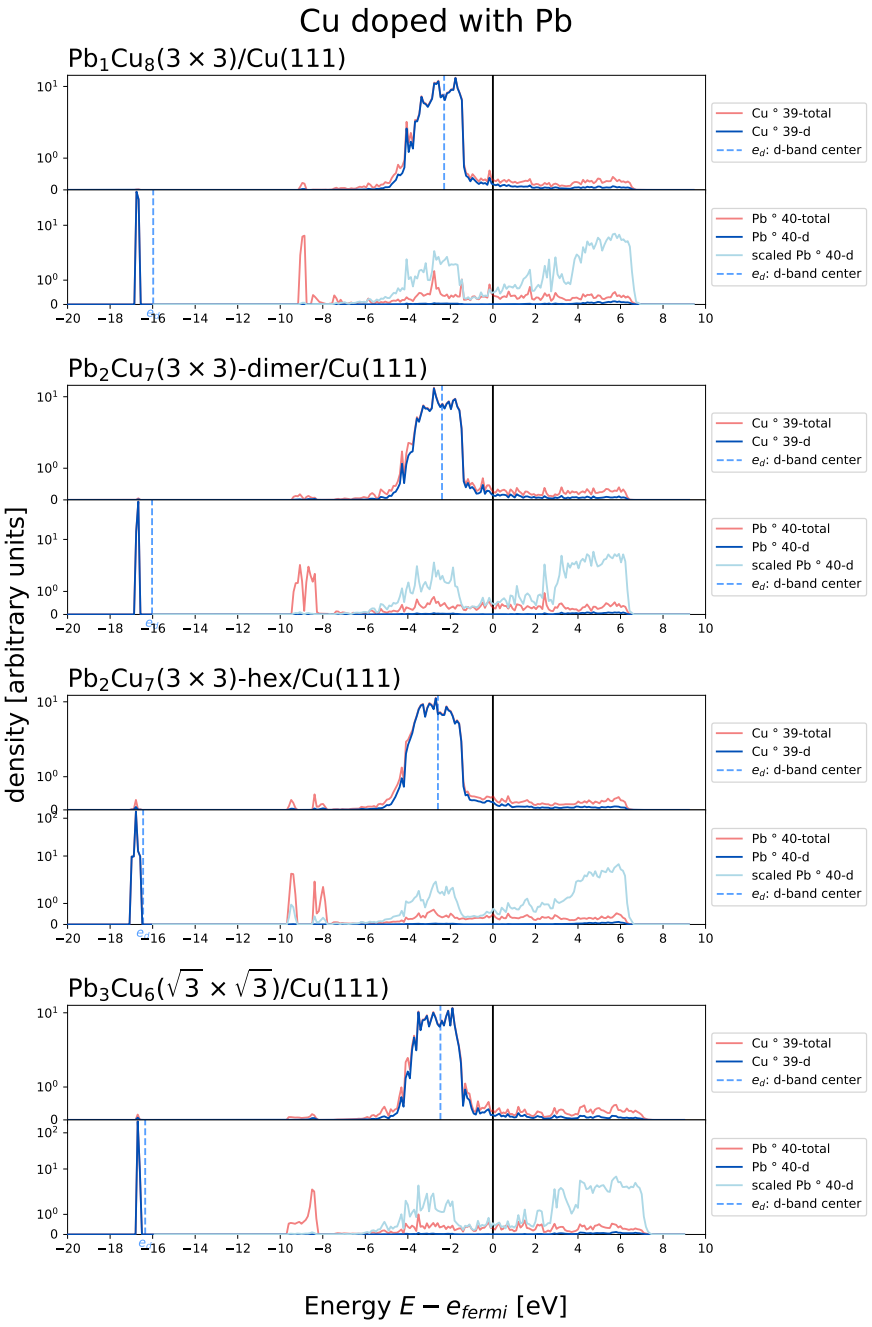


Figure S7: Selection of projected local density of states of the surface alloys of copper doped with lead. The d-band is drawn in blue with the d-band center e_d as a light blue dashed line and an even lighter blue line for a scaled up version of the d-band from -16 eV to 10eV. The scaled up version is only drawn in for lead as its d-band is dominated by the peak between -18eV and -16 eV. The total LDOS of the atom is colored read. The density axis is in symmetrical logarithmic scale, meaning it is logarithmic except for an interval around zero where it is linear.

References

[S1] Bagger, A.; Ju, W.; Varela, A. S.; Strasser, P.; Rossmeisl, J. Electrochemical CO2 Reduction: A Classification Problem. *Chemphyschem Eur. J. Chem. Phys. Phys. Chem.* **2017**, *18*, 3266–3273.

[S2] Chan, K.; Tsai, C.; Hansen, H. A.; Nørskov, J. K. Molybdenum Sulfides and Selenides as Possible Electrocatalysts for CO2 Reduction. *ChemCatChem* **2014**, *6*, 1899–1905.

[S3] Yoo, J. S.; Christensen, R.; Vegge, T.; Nørskov, J. K.; Studt, F. Theoretical Insight into the Trends That Guide the Electrochemical Reduction of Carbon Dioxide to Formic Acid. *ChemSusChem* **2016**, *9*, 358–363.

[S4] Christensen, R.; Hansen, H. A.; Vegge, T. Identifying Systematic DFT Errors in Catalytic Reactions. *Catal. Sci. Technol.* **2015**, *5*, 4946–4949.

[S5] Peterson, A. A.; Abild-Pedersen, F.; Studt, F.; Rossmeisl, J.; Nørskov, J. K. How Copper Catalyzes the Electroreduction of Carbon Dioxide into Hydrocarbon Fuels. *Energy Environ. Sci.* **2010**, *3*, 1311–1315.